

Langmuir, 24 (11), 5961–5966, 2008. 10.1021/la703664r

Web Release Date: April 29, 2008

Copyright © 2008 American Chemical Society

Quantum Dot Micropatterning on Si

K. Lambert,[‡] I. Moreels,[‡] D. Van Thourhout,[‡] and Z. Hens^{*‡}

Physics and Chemistry of Nanostructures, Ghent University, Krijgslaan 281-S12, B-9000 Ghent, Belgium, and Department of Information Technology, Ghent University-IMEC, Sint-Pietersnieuwstraat 41, B-9000 Ghent, Belgium

Received November 23, 2007

Revised Manuscript Received: February 19, 2008

Abstract:

Using InP and PbSe quantum dots, we demonstrate that the Langmuir–Blodgett technique is well-suited to coat nonflat surfaces with quantum dot monolayers. This allows deposition on silicon substrates covered by a developed patterned resist, which results in monolayer patterns with micrometer resolution. Atomic force microscopy and scanning electron microscopy reveal the formation of a densely packed monolayer that replicates predefined structures with high selectivity after photoresist removal. A large variety of shapes can be reproduced and, due to the excellent adhesion of the quantum dots to the substrate, the hybrid approach can be repeated on the same substrate. This final possibility leads to complex, large-area quantum dot monolayer structures with micrometer spatial resolution that may combine different types of quantum dots.

1. Introduction

Research on colloidal nanocrystals has made substantial progress over the past 25 years. Optimized synthesis procedures allow for the production of monodisperse suspensions of metal, metal oxide, and semiconductor nanocrystals over a wide range of materials and sizes.^{1–3} This has led to detailed studies of the optical and electronic properties of colloidal nanocrystals like Au,⁴ CdSe,^{5,6} InAs,⁷ InP,⁸ PbSe,⁹ and many others, often showing excellent agreement with theoretical calculations.^{6,9,10} More recently, several research groups have started taking advantage of the unique nanocrystal properties by implementing them in devices used for a broad range of applications. For example, different colloidal nanocrystals have been successfully incorporated in efficient nanocrystal light-emitting devices^{11–15} and in field-effect transistors,¹⁶ while Au nanocrystals have been used as catalysts for nanowire growth¹⁷ or in sensing applications.¹⁸

Such implementation often requires deposition of a thin film or a monolayer of nanocrystals on top of a glass, indium tin oxide, or metallic substrate. Typically, this is achieved by techniques like drop-casting,¹⁹ spin-coating,^{11,14,20} Langmuir–Blodgett (LB) deposition,^{21–25} or self-assembly onto substrates derivatized with bifunctional molecules.^{26–28} Although convenient, these techniques offer little or no control over the geometry and position of the deposited layer on the substrate, which may limit the practical development and miniaturization of devices based on colloidal nanocrystals. Up till now, micropatterning has been realized using approaches like LB deposition of single-particle lines,¹⁷ electrophoretic deposition,²⁹ or lithography of a thin film of colloidal nanocrystal dispersed in poly(methyl methacrylate).³⁰ However, a general method for micropatterning of colloidal nanocrystal monolayers or thin films is not available yet.

Using colloidal InP quantum dots (Q-InP), passivated with short-chain ligand molecules such as pentamethylene sulfide (Q-InP/PMS) and pyridine (Q-InP/PYR), and PbSe quantum dots passivated with oleic acid (Q-PbSe), we first demonstrate that the LB technique is not only applicable to a flat silicon substrate, but can also be used to coat various 3D photonic structures. We then propose an approach based on a combination of LB deposition of quantum dots on silicon and optical lithography to overcome the problem stated above. It leads to micropatterning of nanocrystal monolayers with micrometer resolution. Deposited structures are robust enough to enable the fabrication of complex structures via successive depositions.

2. Experimental Section

2.1. InP Quantum Dots. Nearly monodisperse InP nanocrystals ($\sigma < 10\%$) were synthesized and size-selected according to literature methods.^{31,32} To establish the relation between the wavelength of the exciton absorption and the quantum dot diameter, we used transmission electron microscopy (TEM) and UV–vis absorption spectroscopy, and published extinction coefficients were used to determine the nanocrystal concentration.³³ After synthesis, the trioctylphosphine oxide (TOPO) capping of the Q-InP was substituted by pyridine (PYR) or pentamethylene sulfide (PMS) in order to obtain a short and rigid capping layer. Details of the exchange procedure are discussed elsewhere.^{24,34} After ligand exchange, Q-InP/PMS and Q-InP/PYR nanocrystals were suspended in a 1:1 mixture of chloroform and isopropanol.

2.2. PbSe Quantum Dots. Monodisperse colloidal PbSe nanocrystals with a mean diameter of 5.4 nm ($\sigma < 5\%$) were synthesized using an optimized version of the synthesis described by Murray and co-workers.¹ More details about the synthesis are given elsewhere.³⁵ The nanocrystals are capped with oleic acid and are suspended in chloroform.

2.3. Monolayer Deposition. Single monolayers of Q-InP/PMS, Q-InP/PYR or Q-PbSe were deposited on silicon substrates and silicon-on-insulator (SOI) photonic structures (waveguides, ring resonators, etc.) with a Nima 312D LB trough. Typically, we placed the substrate vertically in the trough, after which a few drops (25–100 μL) of a quantum dot suspension were spread out on a water surface (200 cm^2). Deionized water with a resistivity above 5 $\text{M}\Omega/\text{cm}$ was used. For Q-InP, parameters of a published procedure²⁴ have been used without alterations: a close-packed monolayer of nanocrystals was formed after solvent evaporation by successive compression and expansion of the film at a rate of 50 cm^2/min up to a surface pressure of 20 mN/m . For Q-PbSe, one compression at a rate of 10 cm^2/min was used. The monolayer was transferred to the substrate by vertically pulling the substrate out of the trough at a speed of 1–5 mm/min and a constant surface pressure of 20 mN/m .

2.4. Micropatterning. Local monolayer deposition started with spin-coating a 1 μm thick Clariant AZ 5214 E Novolak photoresist film on silicon (Figure 1a) or SOI substrates, which was subsequently patterned by optical lithography (Figure 1b). On this patterned substrate, a quantum dot monolayer was deposited with the LB technique as described above (Figure 1c). After deposition, the resist was removed by subsequently dipping the sample in acetone (60 s), isopropanol (45 s), and distilled water (30 s) in the case of Q-InP/PMS and Q-PbSe, and isopropanol (5 min), acetone (30 s), and distilled water (15 s) in the case of Q-InP/PYR (Figure 1d). Multiple depositions were obtained by simply repeating the entire procedure on the same substrate.



Figure 1. Principle of the micropatterning technique. (a) Spin-coating of a photoresist onto a silicon substrate. (b) Pattern definition in the photoresist. (c) Langmuir deposition on the substrate. (d) Dissolution of the photoresist.

[Click to Enlarge](#)

2.5. Characterization. The quality of the substrates and deposited layers was assessed with a variety of characterization methods at different stages during the process. Scanning electron microscopy (SEM) measurements were performed with a FEI Quanta 200 F SEM and a FEI Nova 600 Nanolab Dual-Beam focused ion beam in secondary electron mode. Atomic force microscopy (AFM) analysis was done with a Molecular Imaging PicoPlus system, in AC AFM mode. TEM samples were prepared by holding a carbon-coated copper grid between a pair of tweezers and briefly letting the grid touch the nanocrystal film on the LB trough. The samples were examined using a Jeol 2200 FS microscope.

3. Results and discussion

3.1. LB Deposition on Silicon. 3.1.1. InP. Previous results on mica substrates have demonstrated that the use of PMS ligands improves the homogeneity of Q-InP nanocrystal LB monolayers. When deposited at a surface pressure of 20 mN/m, these layers contain few holes and almost no nanocrystals on top of the monolayer.²⁴ Using the same procedure, similar results were obtained on a silicon substrate. Figure 2a indicates that nanocrystal grains may form, with small voids separating the different islands. At the grain boundaries, the monolayers may overlap, forming small nanocrystal stacks with a height corresponding to the size of two or three nanocrystals.

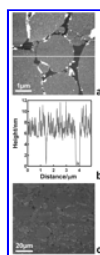


Figure 2. Results of the LB deposition of a Q-InP/PMS monolayer on a silicon substrate. (a) AFM image showing formation of nanocrystal grains, with stacks of Q-InP/PMS at the grain boundaries. (b) Profile of (a). Two levels can be observed, with a height difference of 5.5 nm. The lower level corresponds to the silicon substrate, and the higher level is attributable to the Q-InP/PMS monolayer. (c) SEM image of a Q-InP/PMS monolayer. At large scales, the grains and grain boundaries can be observed.

[Click to Enlarge](#)

Figure 2b shows a height profile of Figure 2a. Two distinct levels can be observed, the lowest corresponding to the dark voids in the AFM image, and the highest corresponding to the islands. The height difference between both levels (5.5–6 nm) is comparable to the diameter of the Q-InP/PMS, 5.2 nm when taking the thickness of the PMS capping layer (0.3 nm) into account. As the lower level is as flat as bare Si, we conclude that we deposited a monolayer of Q-InP/PMS, where the voids correspond to the Si substrate and the islands to the Q-InP/PMS monolayer.

To evaluate the monolayer quality over larger areas, we compared the AFM results with SEM images. Both images show the monolayer as gray islands on a dark background, which represents the bare substrate. The multilayer areas appear as lighter tones. This means that we can use SEM to examine the monolayer quality on a far larger scale than accessible by AFM. From the SEM image, we can conclude that the nanocrystal monolayer is composed of 2D grains that can be as large as $20 \times 20 \mu\text{m}^2$, with nanocrystal stacks at the edges.

On a smaller scale, TEM images of Q-InP|PYR films reveal the arrangement of the individual nanocrystals in the Langmuir films. We see formation of close-packed films, although with no long-range hexagonal symmetry (Figure 3b). In the case of Q-InP|PMS, preparation of good Langmuir film TEM samples proved to be more difficult. The films still appear as close packed but show more hole defects. The fact that these are not observed with AFM or SEM suggests that Q-InP|PMS films are more easily damaged during TEM sample preparation.

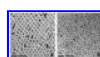


Figure 3. TEM images of LB monolayers of Q-PbSe (a) and Q-InP (b).

[Click to Enlarge](#)

3.1.2. PbSe. Q-PbSe monolayers deposited on flat silicon and mica do not contain the imperfections mentioned above for Q-InP layers: the films are void- and multilayer-free over ranges of tens of micrometers. The absence of imperfections and thus contrast makes the Q-PbSe films difficult to image using AFM and SEM. Therefore, only images of the patterned monolayers will be shown in this paper. TEM images (Figure 3a), however, confirm that a monolayer of Q-PbSe is formed. As with Q-InP, the monolayer exhibits only local hexagonal symmetry.

Typical surface pressure–surface area isotherms obtained during LB deposition of Q-InP|PMS, Q-InP|PYR, and Q-PbSe films on silicon are briefly discussed in the [Supporting Information](#).

3.2. LB deposition on SOI structures. Unlike other coating techniques such as drop-casting and spin-coating, the LB technique may allow conformal layer deposition on nonflat substrates. We demonstrate this by coating SOI structures with Q-InP|PMS monolayers, as the inherent imperfections and thus contrast between the Q-InP monolayers and the substrate makes it easier to study the results of the deposition process. The same parameters as for flat silicon were used. Figure 4 shows the results of a LB deposition on photonic wires of constant height (300 nm) but variable width. By means of its defects, one sees that in Figure 4a the monolayer follows the complete structure and coats the substrate and the top of the waveguides. Conformal sidewall coating is suggested by the continuation of the defect patterns in Figure 4a and is clearly demonstrated by the tilted SEM image in Figure 4c (indicated by the circle). Whereas the top of the wires is generally well coated, more imperfections are found at the bottom of the structures: the cracks indicated by the arrows in Figure 4c suggest that it is difficult to bend the layer over 90° . Additionally, between parallel waveguides with a spacing of a few micrometers, cracks parallel to these structures may occur (indicated by the ellipse in Figure 4c). The smallest structures (500 nm wide wires, Figure 4c) occasionally show a loss in homogeneity, probably due to the limited width of the wire, although the overall coverage remains good. Only at very narrow (250 nm) gaps in between two wires, we found that the deposition becomes systematically inhomogeneous. In a similar way, more complex structures, containing photonic wires in various directions, were coated as well. As all sides in such structures exhibit an identical coating quality, we can conclude that the deposition is essentially orientation independent.

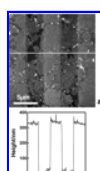


Figure 4. Results of LB deposition of a Q-InP|PMS monolayer on SOI structures. (a–b) AFM image of a coated 3 μm wide photonic waveguide (a) with corresponding height profile along the grey line (b). The islands continue across the wire edges. (c) SEM image of coated 500 nm wide photonic wires. The monolayer smoothly follows the complete structure (indicated by circle), although the layer is systematically cracked at the bottom of the structures (indicated by the grey arrows) and cracks parallel to the wires may occur (indicated by ellipse).

[Click to Enlarge](#)

3.3. Micropatterning on Silicon. 3.3.1. Q-InP. Integration of colloidal nanocrystals in various devices will often require deposition of particles at very specific places on a substrate. As the LB technique allows deposition of a homogeneous monolayer on 3D structures, we choose an approach to obtain local deposition involving LB deposition on a substrate coated with developed photoresist, as explained in Figure 1. Figure 5a shows that the Q-InP/PMS monolayer forms a continuous layer across the photoresist boundary, undisturbed by the sudden height difference due to the photoresist. After photoresist dissolution, the nanocrystal monolayer strongly contrasts with the recovered bare silicon substrate (Figure 5b). This demonstrates that efficient coverage of a photoresist patterned substrate with a monolayer is possible and the nanocrystals deposited on the photoresist can be completely removed without affecting those on the silicon substrate. This high selectivity indicates that the film adherence through particle–substrate and interparticle van der Waals interactions is strong enough to withstand extensive and repeated wet processing, as demonstrated before by the LB deposition of single particle line patterns.¹⁷ It also indicates that, although acetone does not form stable Q-InP/PMS colloidal suspensions, there is sufficient stabilization of the removed nanocrystals to prevent immediate redeposition onto the substrate during the resist dissolution process.

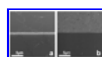


Figure 5. Result of Q-InP/PMS monolayer deposition before (a) and after (b) photoresist removal. Before removal, the monolayer extends continuously over the edge of the resist (a, bottom half). After removal, we observed that the pattern is well replicated by the monolayer (so the monolayer on silicon remains unaffected by the dissolution process), while there is a good removal of the monolayer that was on top of the photoresist (b, bottom half).

[Click to Enlarge](#)

A large variety of patterns was used to assess the capabilities of the deposition technique. Squares of sizes from $200 \times 200 \mu\text{m}^2$ down to $10 \times 10 \mu\text{m}^2$ in the initial photoresist pattern are all well replicated (Figure 6a). Reduction of the size to $5 \times 5 \mu\text{m}^2$ is possible (Figure 6b), although defects were observed on some of these smaller structures. Moreover, deposition is not limited to square or rectangular patterns: angles from 60° up to 320° all can be filled with high accuracy (Figure 6c–d). In practice, this means that the approach allows for substantial freedom in pattern design. Patterns of almost any shape can be replicated by the Q-InP/PMS monolayer, and the filling of the patterns does not depend on the substrate orientation during the LB deposition: top, bottom, left, and right are indistinguishable in all images. In Figure 6e, the accuracy of the process is further demonstrated by two covered areas separated by a monolayer-free $2 \mu\text{m}$ strip. Hence, a high density of covered, yet well-separated, areas can be made.

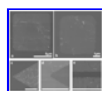


Figure 6. SEM images of micropatterning of Q-InP/PMS monolayers, using patterned photoresist. (a–b) Squares as small as $10 \times 10 \mu\text{m}^2$ (a) are replicated with high precision and selectivity, and even $5 \times 5 \mu\text{m}^2$ squares (b) could be made. (c–d) Acute (60°) up to reflex angles (320°) all are well replicated. (e) Covered areas can be separated by a zone only $2 \mu\text{m}$ wide. The scale bar represents $10 \mu\text{m}$ (c–e).

[Click to Enlarge](#)

3.3.2. Q-PbSe. Similar results were obtained with Q-PbSe (Figure 7a). However, because of the excellent homogeneity of the PbSe films, a clear effect of the resist thickness on the deposition quality could be observed. Figure 7 shows fragments of a linear Q-PbSe patterns made with thin (76 nm , b) and thick (1500 nm , c) photoresist, where other deposition parameters remained unchanged. The resist thickness clearly influences the film homogeneity: the 1500 nm resist results in monolayers with tears, whereas the 76 nm resist enables deposition of undamaged monolayers. This suggests that larger height differences cause more stress in the monolayer during the deposition process, imposing a limit on the height of the 3D objects that can be coated with the LB technique. Also, the thin resist often led to cleaner uncoated areas, although at the moment it is not clear why. In contrast with similar InP-based samples, the PbSe patterns exhibit a distinct border with approximately twice the monolayer height and a width proportional to the resist thickness. Height profiles of Figure 7b and c, showing that the pattern consists of a Q-PbSe monolayer, are given in the [Supporting Information](#).

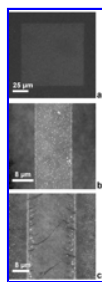


Figure 7. SEM image of a patterned Q-PbSe monolayer (a) and AFM images of patterned monolayers using resist with a thickness of 76 nm (b) and 1500 nm (c).

[Click to Enlarge](#)

3.3.3. Resist Dissolution. Control over the resist dissolution is a crucial step in the monolayer micropatterning scheme we propose. Although the experiments with Q-PbSe clearly show that thin photoresist films give better results, a minimum resist thickness is required for efficient patterning. Moreover, this not only depends on the quantum dot type, but also on the quantum dot ligands. For example, whereas acetone is an adequate solvent for resist dissolution in order to obtain Q-InP/PMS or Q-PbSe patterns, this gave poor results with Q-InP/PYR. Large parts (tens to hundreds of square micrometers) of the monolayer on the resist were redeposited irreversibly on the silicon substrate during resist dissolution. Although this kind of attachment is unwanted, it is indicative of the strong interparticle and film–substrate interactions that make the monolayer patterning procedure possible. Using a $1 \mu\text{m}$ thick resist, the undesired attachment could be avoided by performing a more gentle dissolution of the photoresist in isopropanol instead of fast dissolution in acetone, yielding similar results as obtained with Q-InP/PMS. With the thin resist, the unwanted attachment could not be avoided.

3.4. Successive Patterning. Since processing does not affect the integrity of the monolayer structures, the process may lend itself to multiple depositions. To evaluate this, we covered silicon substrates with a patterned resist containing parallel lines with widths ranging from 10 to $50 \mu\text{m}$. After Q-InP/PYR monolayer deposition and resist dissolution, this process was repeated with the same pattern rotated over 90° . SEM (Figure 8b) and AFM measurements on such structures (Figure 8a) clearly show perpendicular monolayer lines, which overlap at the crossing. This implies that our technique allows independent deposition of monolayers of nanocrystals of different sizes or properties, resulting in robust and complex structures. This kind of quantum dot monolayer micropatterning on a flat substrate complies with the requirements of several applications, like for example light-emitting or photovoltaic devices.¹¹



Figure 8. AFM (a) and SEM (b) image of multiple depositions of InP QD monolayer structures on silicon. The scale of the AFM image is $50 \mu\text{m} \times$

50 μm \times 8 nm.

[Click to Enlarge](#)

3.5. Resolution. The resolution of the hybrid approach we propose for micropatterning of QD monolayers depends on factors like LB film quality, lithographic resolution, quality of 3D coating, resist dissolution, and resist thickness.

The quality of the LB films depends on the deposition parameters and on the type of nanocrystals used. As shown in Figure 2, Q-InP/PMS films may contain voids extending over 1 μm or more, which means that replication of monolayer structures of these dimensions can not be fully ensured. This makes film quality an important resolution-limiting factor for the deposition of monolayer microstructures. Taking the example of the monolayer strips (Figure 8), it is clear that voids will hamper the deposition of continuous strips with a width smaller than a few micrometers. We find that 10 μm strips can be deposited without difficulties, while more narrow strips (5 μm or less) may be interrupted at some places. Similar conclusions hold for the square patterns shown in Figure 6: 10 \times 10 μm^2 squares are well replicated, whereas 5 \times 5 μm^2 squares may show imperfections due to holes.

In terms of substrate geometry, LB deposition on a resist-coated substrate is similar to deposition on waveguide structures. Therefore, an assessment of the resolution achievable with perfect LB films is possible using the results of LB deposition on SOI structures. As demonstrated by Figure 4a and b, a 2.5 μm gap in between two waveguides can be coated, while homogeneity is completely lost with a 0.25 μm gap. This means that with high quality LB films, monolayer patterns with sizes of 1 μm or more can be made using our photolithography-based approach. On the other hand, patterns with features of a few hundred nanometers will be hard to achieve. Hence, the lack of conformal coating of sub-micrometer gaps or holes in the photoresist will probably limit the resolution of monolayer patterns made from defect-free LB films.

Another parameter that may introduce defects is the resist thickness. As demonstrated with Q-PbSe, the photoresist layer should be kept thin to maintain defect-free patterns. On the other hand, thin resist layers may complicate the efficient removal of particles during resist dissolution. We found that the minimum resist thickness necessary for patterning varies with the type of quantum dots and the nature of the ligands.

In contrast with monolayer microstructures, the resolution of monolayer-free patterns (blank areas between monolayer patterns) depends less on LB film quality. As shown by Figure 6e, large-area quantum dot monolayers can be neatly separated by a 2 μm nanocrystal-free strip. Moreover, since 0.5 μm wide waveguides can be coated homogeneously (Figure 6a), we expect that sub-micrometer resolution is well possible with monolayer-free patterns. Therefore, lithographic limitations rather than loss of conformal coating on 3D substrates may limit resolution in the case of monolayer-free patterns.

4. Conclusion

By coating 3D SOI structures with Q-InP and Q-PbSe monolayers, we show that the LB technique applies both to flat and nonflat substrates. The deposited layers smoothly follow structures with dimensions down to 500 nm, and only at narrow gaps (250 nm) in between structures homogeneous deposition was impossible. Especially for Q-PbSe, such micropatterned coatings on SOI structures are relevant, since its bandgap and luminescence can be adapted to telecommunication wavelengths.

Using silicon substrates coated with a developed photoresist film instead of SOI structures, successful quantum dot monolayer micropatterning is achieved. This hybrid approach is independent of substrate orientation and gives access to a large flexibility in pattern design. Large (200 \times 200 μm^2) and small (10 \times 10 μm^2) areas, and acute up to reflex angles can be replicated with high accuracy. In the case of Q-InP, the resolution of monolayer patterns is governed mainly by the quality of the Langmuir film. The voids in the film limit the technique to structures down to 5–10 μm . The resolution of monolayer-free patterns is better, as it depends less on LB film quality. Monolayer-free patterns of 2 μm have been obtained, but sub-micrometer resolution is expected to be possible, as 3D structures of 500 nm can be coated homogeneously.

In addition to the selectivity and precision of the technique, the good adhesion of the quantum dots to the substrate allows successive depositions on the same substrate, yielding robust and complex monolayer patterns that combine QDs of different sizes and, thus, different properties.

The fact that a change of ligands or even different types of quantum dots only requires minor changes in the procedure demonstrates the flexibility of the technique. This suggests that the presented methods can be extended to other colloidal materials and substrates and could even allow for deposition of different materials in separated areas of the same substrate. Therefore, we believe that this combination of LB deposition and optical lithography could be a valuable contribution to the development of novel devices based on colloidal QD microstructures.

Acknowledgment

The authors thank the Institute for the Promotion of Innovation through Science and Technology in Flanders (IWT-Vlaanderen) for a scholarship (I.M.) and Belgian Science Policy for a research grant (Z.H., IAP 6/10, Photonics@be). Steven Verstuyft (Intec, UGent) is acknowledged for performing the photolithography on our samples.

Supporting Information Available

Surface pressure–surface area isotherms for Q-InP/PMS, Q-InP/PYR, and Q-PbSe monolayer deposition and height profiles of the AFM images in Figure 7b and c. This information is available free of charge via the Internet at <http://pubs.acs.org>.

* To whom correspondence should be addressed. E-mail: Zeger.Hens@UGent.be.

† Physics and Chemistry of Nanostructures, Ghent University.

‡ Department of Information Technology, Ghent University-IMEC.

1. Murray, C. B.; Sun, S. H.; Gaschler, W.; Doyle, H.; Betley, T. A.; Kagan, C. R. *IBM J. Res. Dev.* **2001**, *45*, 47–56. [[ChemPort](#)]
2. Green, M. *Curr. Opin. Solid State Mater. Sci.* **2002**, *6*, 355–363. [[ChemPort](#)] [[CrossRef](#)]
3. Masala, O.; Seshadri, R. *Ann. Rev. Mater. Res.* **2004**, *34*, 41–81. [[ChemPort](#)] [[CrossRef](#)]
4. Link, S.; El-Sayed, M. A. *J. Phys. Chem. B* **1999**, *103*, 8410–8426. [[Full Text - ACS](#)] [[ChemPort](#)] [[CrossRef](#)]
5. Norris, D. J.; Bawendi, M. G. *Phys. Rev. B* **1996**, *53*, 16338–16346. [[ChemPort](#)] [[CrossRef](#)]
6. Bakkers, E.P.A.M.; Hens, Z.; Zunger, A.; Franceschetti, A.; Kouwenhoven, L. P.; Gurevich, L.; Vanmaekelbergh, D. *Nano Lett.* **2001**, *1*, 551–556. [[Full Text - ACS](#)] [[ChemPort](#)] [[CrossRef](#)]
7. Banin, U.; Cao, Y. W.; Katz, D.; Millo, O. *Nature* **1999**, *400*, 542–544. [[ChemPort](#)] [[CrossRef](#)]

8. Micic, O. I.; Cheong, H. M.; Fu, H.; Zunger, A.; Sprague, J. R.; Mascarenhas, A.; Nozik, A. J. *J. Phys. Chem. B* **1997**, *101*, 4904–4912. [[Full Text - ACS](#)] [[ChemPort](#)] [[CrossRef](#)]
9. Liljeroth, P.; van Emmichoven, P. A. Z.; Hickey, S. G.; Weller, H.; Grandidier, B.; Allan, G.; Vanmaekelbergh, D. *Phys. Rev. Lett.* **2005**, *95*, 086801. [[ChemPort](#)] [[Medline](#)] [[CrossRef](#)]
10. An, J. M.; Franceschetti, A.; Dudiy, S. V.; Zunger, A. *Nano Lett.* **2006**, *6*, 2728–2735. [[Full Text - ACS](#)] [[ChemPort](#)] [[Medline](#)] [[CrossRef](#)]
11. Coe, S.; Woo, W. K.; Bawendi, M.; Bulovic, V. *Nature* **2002**, *420*, 800–803. [[ChemPort](#)] [[Medline](#)] [[CrossRef](#)]
12. Coe-Sullivan, S.; Steckel, J. S.; Woo, W. K.; Bawendi, M. G.; Bulovic, V. *Adv. Funct. Mater.* **2005**, *15*, 1117–1124. [[ChemPort](#)] [[CrossRef](#)]
13. Sargent, E. H. *Adv. Mater.* **2005**, *17*, 515–522. [[ChemPort](#)] [[CrossRef](#)]
14. Chaudhary, S.; Ozkan, M.; Chan, W. C. W. *Appl. Phys. Lett.* **2004**, *84*, 2925–2927. [[ChemPort](#)] [[CrossRef](#)]
15. O'Connor, E.; O'Riordan, A.; Doyle, H.; Moynihan, S.; Cuddihy, A.; Redmond, G. *Appl. Phys. Lett.* **2005**, *86*, 201114. [[CrossRef](#)]
16. Talapin, D. V.; Murray, C. B. *Science* **2005**, *310*, 86–89. [[ChemPort](#)] [[Medline](#)] [[CrossRef](#)]
17. Huang, J. X.; Tao, A. R.; Connor, S.; He, R. R.; Yang, P. D. *Nano Lett.* **2006**, *6*, 524–529. [[Full Text - ACS](#)] [[ChemPort](#)] [[Medline](#)] [[CrossRef](#)]
18. Nath, N.; Chilkoti, A. *Anal. Chem.* **2002**, *74*, 504–509. [[Full Text - ACS](#)] [[ChemPort](#)] [[Medline](#)] [[CrossRef](#)]
19. Lin, X. M.; Jaeger, H. M.; Sorensen, C. M.; Klabunde, K. J. *J. Phys. Chem. B* **2001**, *105*, 3353–3357. [[Full Text - ACS](#)] [[ChemPort](#)] [[CrossRef](#)]
20. Roither, J.; Heiss, W.; Talapin, D. V.; Gaponik, N.; Eychmuller, A. *Appl. Phys. Lett.* **2004**, *84*, 2223–2225. [[ChemPort](#)] [[CrossRef](#)]
21. Meldrum, F. C.; Kotov, N. A.; Fendler, J. H. *Langmuir* **1994**, *10*, 2035–2040. [[Full Text - ACS](#)] [[ChemPort](#)] [[CrossRef](#)]
22. Gattas-Asfura, K. M.; Constantine, C. A.; Lynn, M. J.; Thimann, D. A.; Ji, X. J.; Leblanc, R. M. *J. Am. Chem. Soc.* **2005**, *127*, 14640–14646. [[Full Text - ACS](#)] [[ChemPort](#)] [[Medline](#)] [[CrossRef](#)]
23. Ferreira, P. M. S.; Timmons, A. B.; Neves, M. C.; Dynarowicz, P.; Trindade, T. *Thin Solid Films* **2001**, *389*, 272–277. [[ChemPort](#)] [[CrossRef](#)]
24. Lambert, K.; Wittebrood, L.; Moreels, I.; Deresmes, D.; Grandidier, B.; Hens, Z. *J. Colloid Interface Sci.* **2006**, *300*, 597–602. [[ChemPort](#)] [[Medline](#)] [[CrossRef](#)]
25. Dabbousi, B. O.; Murray, C. B.; Rubner, M. F.; Bawendi, M. G. *Chem. Mater.* **1994**, *6*, 216–219. [[Full Text - ACS](#)] [[ChemPort](#)] [[CrossRef](#)]
26. Nakanishi, T.; Ohtani, B.; Uosaki, K. *J. Phys. Chem. B* **1998**, *102*, 1571–1577. [[Full Text - ACS](#)] [[ChemPort](#)] [[CrossRef](#)]
27. Colvin, V. L.; Goldstein, A. N.; Alivisatos, A. P. *J. Am. Chem. Soc.* **1992**, *114*, 5221–5230. [[Full Text - ACS](#)] [[ChemPort](#)] [[CrossRef](#)]
28. Bethell, D.; Brust, M.; Schiffrin, D. J.; Kiely, C. J. *Electroanal. Chem.* **1996**, *409*, 137–143. [[CrossRef](#)]
29. Gao, M. Y.; Sun, J. Q.; Dulkeith, E.; Gaponik, N.; Lemmer, U.; Feldmann, J. *Langmuir* **2002**, *18*, 4098–4102. [[Full Text - ACS](#)] [[ChemPort](#)] [[CrossRef](#)]
30. Martiradonna, L.; Stomeo, T.; De Giorgi, M.; Cingolani, R.; De Vittorio, M. *Microelectron. Eng.* **2006**, *83*, 1478–1481. [[ChemPort](#)] [[CrossRef](#)]
31. Guzelian, A. A.; Katari, J. E. B.; Kadavanich, A. V.; Banin, U.; Hamad, K.; Juban, E.; Alivisatos, A. P.; Wolters, R. H.; Arnold, C. C.; Heath, J. R. *J. Phys. Chem.* **1996**, *100*, 7212–7219. [[Full Text - ACS](#)] [[ChemPort](#)] [[CrossRef](#)]
32. Micic, O. I.; Sprague, J. R.; Curtis, C. J.; Jones, K. M.; Machol, J. L.; Nozik, A. J.; Giessen, H.; Fluegel, B.; Mohs, G.; Peyghambarian, N. *J. Phys. Chem.* **1995**, *99*, 7754–7759. [[Full Text - ACS](#)] [[ChemPort](#)] [[CrossRef](#)]
33. Talapin, D. V.; Gaponik, N.; Borchert, H.; Rogach, A. L.; Haase, M.; Weller, H. *J. Phys. Chem. B* **2002**, *106*, 12659–12663. [[Full Text - ACS](#)] [[ChemPort](#)] [[CrossRef](#)]
34. Hens, Z.; Moreels, I.; Martins, J. C. *Chem. Phys. Chem.* **2005**, *6*, 2578–2584. [[ChemPort](#)]
35. Moreels, I.; Lambert, K.; De Muynck, D.; Vanhaecke, F.; Poelman, D.; Allan, G.; Hens, Z. *Chem. Mater.* **2007**, *19*, 6101–6106. [[Full Text - ACS](#)] [[ChemPort](#)] [[CrossRef](#)]